4

Refinement of Protein Tertiary Structure by Using Spin-Spin Coupling Constants from Nuclear Magnetic Resonance Measurements

Jürgen M. Schmidt[1] and Frank Löhr[2]
[1]*School of Biosciences, University of Kent, Canterbury, Kent*
[2]*Institute of Biophysical Chemistry, Center for Biomolecular Magnetic Resonance, Goethe-University, Frankfurt am Main*
[1]*United Kingdom*
[2]*Germany*

1. Introduction

Modelling protein structure seems a challenging enterprise because the number of structure parameters required ordinarily exceeds the amount of independent data points available from experimental observations. Expressing the *predominant conformation* of a protein in terms of a *geometry model*, a polypeptide chain consisting of N atoms would command $3N - 6$ Cartesian coordinates be fixed. Even for small proteins, this becomes a daunting number. Fortunately, so-called holonomic constraints limit the number of variables, leaving substantially fewer, truly relevant parameters for folding the polypeptide chain into its native tertiary structure. For example, adjusting bond lengths and the many angles between the covalent bonds connecting the atoms is of little concern and appropriate standard values can be inserted from tableworks (Pople & Gordon, 1967; Engh & Huber, 1991, 2006). Table 1 exemplifies for the 147-residue protein *Desulfovibrio vulgaris* flavodoxin how the number of truly independent *internal rotational degrees of freedom* amounts to less than one-tenth of the Cartesian coordinate set size.

IUPAC-IUB conventions (1970) define three mainchain torsions for the polypeptide backbone. Protein structure determination primarily seeks to adjust the values of those two mainchain torsion angles that chiefly determine the fold of the chain, that is, ϕ and ψ in each amino-acid residue. Peptide-bond geometry, as described by mainchain torsion angle ω, is normally assumed to be *trans*- or *cis*-planar, fixed at 180° or 0° angles, respectively, and thus does not give rise to rotational variability. In a next instance, the sidechain torsion angle χ_1 is of interest.

Nuclear magnetic resonance (NMR) spectroscopy is uniquely positioned to help determine internal orientational constraints in a molecule, be these atom-atom distances (Wüthrich, 1986; Neuhaus & Williamson, 1989), relative bond orientations (Reif et al., 1997, 2000;

Schwalbe et al., 2001), relative protein domain orientations (Tjandra & Bax, 1997; Fischer et al., 1999) or rotational states of torsion angles (Pachler, 1963, 1964; Hansen et al., 1975; Bystrov, 1976; Ejchart, 1999). Especially powerful at measuring short-range interaction, NMR thus complements X-ray crystallography that is stronger at determining correlations over longer distances.

Approach	Parameters	Items	Coord's
top-down	**Cartesian coordinates** ($3N - 6$)		**6411**
	less bond length constraints ($N - 1$)	– 2138	4273
	less bond angle constraints		
	– at **tetrahedral centers** (5 bond angles to fix)	– 417×5	2188
	— N-terminus	(*1*)	
	— mainchain C^{α} (all residues)	(*147*)	
	— sidechain C^{β} (all residues excl Gly)	(*129*)	
	— sidechain C^{γ} (select residues)	(*85*)	
	— sidechain C^{δ} (select residues)	(*47*)	
	— sidechain C^{ε} (Met, Lys) and N^{ζ} (Lys)	(*8*)	
	– at **planar centers** (3 bond angles to fix)	– 450×3	838
	— mainchain N′ and C′ (excl N- but incl C-terminus)	(*293*)	
	— sidechain nitrogen and carbon	(*157*)	
	– at **angled centers** (1 bond angle to fix)	– 24×1	814
	— sidechain hydroxyl / thiol groups / sulfide bonds	(*24*)	
	less fixed or irrelevant torsion angles		
	— mainchain ω of peptide bonds	– 146	668
	— sidechain methyl	– 84	584
	— sidechain amide / guanidinium groups	– 26	558
	— sidechain hydroxyl / thiol groups	– 24	534
	— N-/C-termini	– 2	**532**
bottom-up	**Variable torsion angles of relevance**		
	— mainchain ϕ and ψ ($2R - 2$)	292	292
	— sidechain χ_1 (all residues excl Gly, Ala)	+ 112	404
	— sidechain χ_2 (select residues)	+ 84	488
	— sidechain χ_3 (select residues)	+ 30	518
	— sidechain χ_4 (Arg, Lys, Pro)	+ 14	**532**

Table 1. Coordinate statistics for *D. vulgaris* flavodoxin (R = 147 residues, N = 2139 atoms)

We here focus on *high-field NMR in aqueous solution* which yields best resolution of the protein signals. Concentrated at around 1 mM, the dissolved protein is exposed to strong

fields of 11.7-23.4 T magnetic flux density, giving rise to nominal resonance frequencies in the proton band (^{1}H) of 500-1000 MHz. Other biologically relevant stable isotopes ^{13}C and ^{15}N, respectively, resonate at roughly one-quarter and one-tenth of ^{1}H at a given field.

NMR experiments then consist of radio-frequency pulse trains that generate controlled transitions of spin states (Ernst et al., 1987). These transitions manifest in resonance lines whose spectrum location and detailed shape reveal information about the molecular environment in which the probed atoms are embedded.

Rotatory states of torsion angles are accessible through measurement of so-called *J*-coupling constants which lend NMR signals a splitting fine structure due to bond-electron mediated pair interactions between NMR active nuclei. Put simply, the presence of each neighbouring (coupled) spin splits the resonance line of the observed spin into two. This splitting is field-*in*dependent (hence coupling 'constant') but does depend on local molecular geometry.

Of particular interest to structure determination are three-bond $^3J_{XY}$ coupling constants as their magnitudes relate to dihedral angles subtended by the three covalent bonds connecting the coupled pair of nuclei X and Y, which can be any combination of ^{1}H, ^{15}N, or ^{13}C, prevalent in the topology of the torsion considered (Fig. 1).

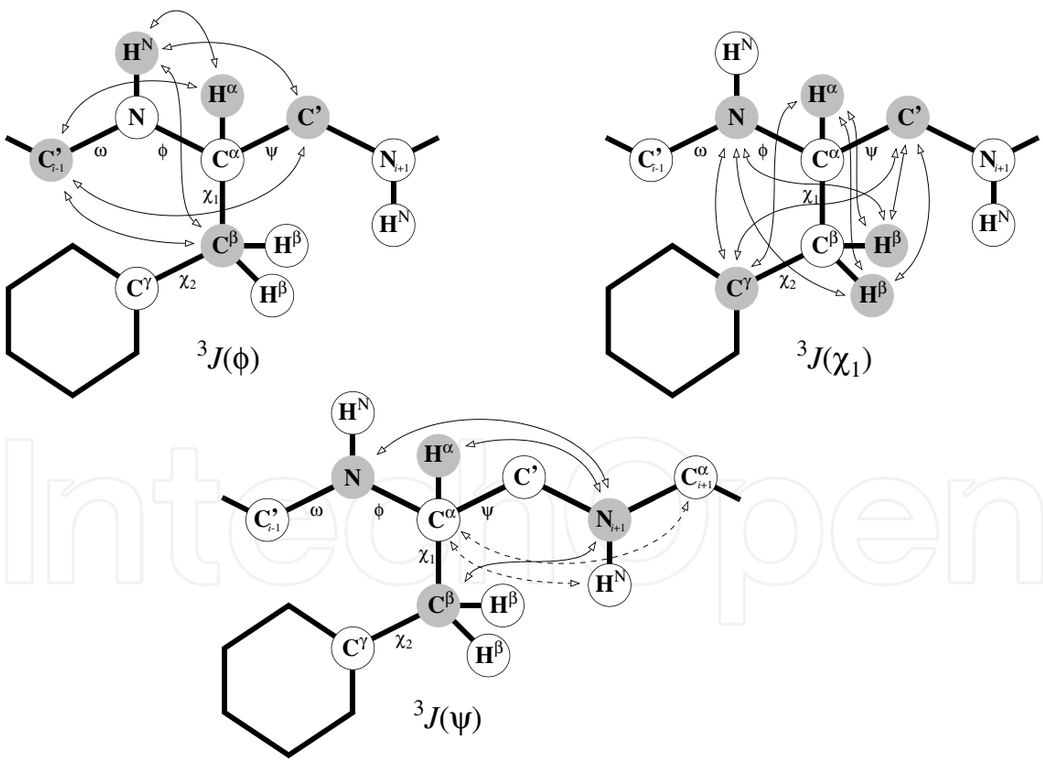

Fig. 1. ^3J spin-spin coupling topologies in ^{13}C,^{15}N enriched polypeptides. Arrows denote three-bond connectivities, grouped by conformational relevance to ϕ, ψ, and χ_1 torsions.

Multiple *J* data collected for a given torsion angle *overdetermine* that angle and thus allow its value to be retrieved. Six coupling constants, $^3J_{HNH\alpha}$, $^3J_{HNC'}$, $^3J_{HNC\beta}$, $^3J_{C'H\alpha}$, $^3J_{C'C'}$, and $^3J_{C'C\beta}$,

determine torsion angle $\phi(C'_{i-1}–N'_i–C^{\alpha}_i–C'_i)$ of residue i (Wang & Bax, 1996; Blümel et al., 1998). Another three couplings, $^3J_{H\alpha N'}$, $^3J_{C\beta N'}$, and $^3J_{N'N'}$, would yield $\psi(N'_i–C^{\alpha}_i–C'_i–N'_{i+1})$. Of qualitative concern only, the planar *trans*- or *cis*-configured peptide bonds at torsion angle $\omega(C^{\alpha}_i–C'_i–N'_{i+1}–C^{\alpha}_{i+1})$ can be verified by two couplings, $^3J_{C\alpha HN}$ and $^3J_{C\alpha C\alpha}$, which appear to reflect ψ geometry also (Hennig et al., 2000). Of numerous sidechain torsions encountered in amino acids, $\chi_1(N'_i–C^{\alpha}_i–C^{\beta}_i–C^{\gamma}_i)$ impacts most on the spatial orientation of the sidechain. Up to nine distinct coupling constants are accessible in amino acids (Pérez et al., 2001).

Karplus (1963) suggested the dependence of ^3J on dihedral angle θ subtended by the three bonds that connect the coupled nuclei follow the empirical relation

$$^3J(\theta) = C_0 + C_1 \cos\theta + C_2 \cos 2\theta \quad (1)$$

where C_m are Karplus coefficients in Hz empirically calibrated for the ^3J types encountered in amino acids (Bystrov, 1976; Wang & Bax, 1995, 1996; Hu & Bax, 1996, 1997; Schmidt et al., 1999, Pérez et al., 2001). Multiples of 60° increments to θ establish the phase relation between the actual internuclear dihedral angle θ and the IUPAC-defined torsion ϕ, ψ, or χ_1 (Fig. 2).

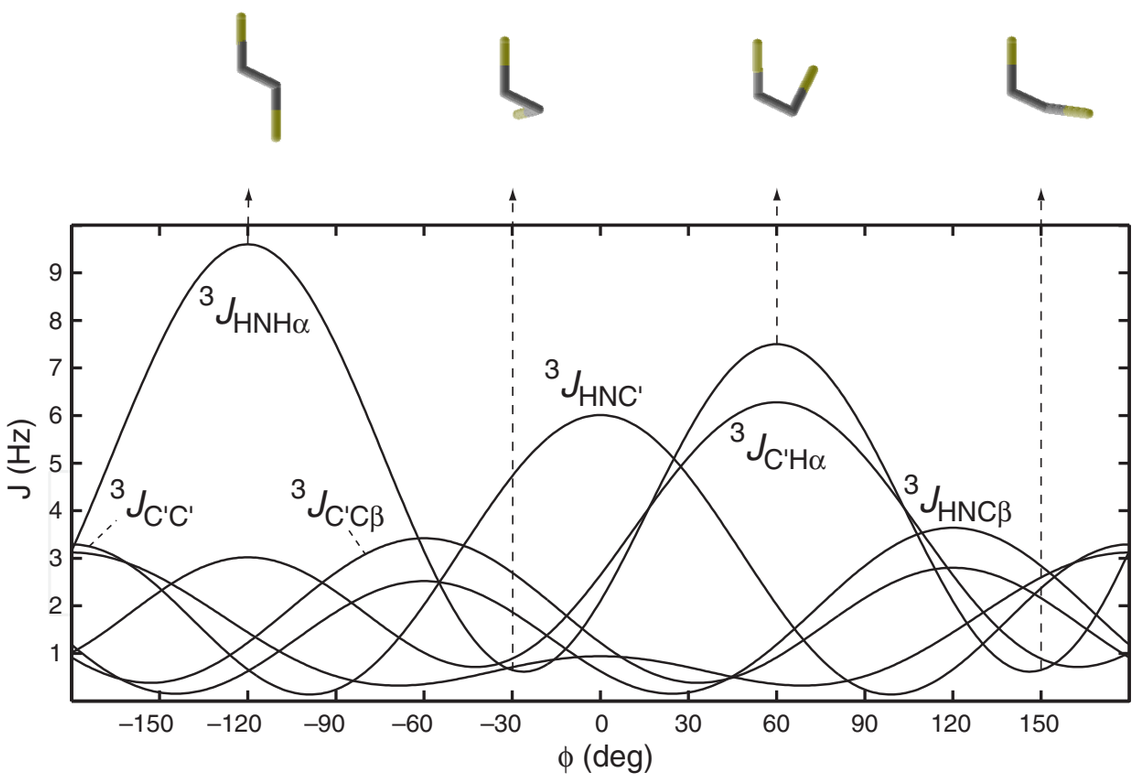

Fig. 2. Angular dependence of the protein ϕ-torsion related ^3J coupling constants. ^3J are at maximum when the bonds between the coupled nuclei are *trans*-oriented, and at minimum for perpendicular orientations. For $^3J_{HNH\alpha}$, the panels show from left to right the internuclear angle $\theta_{HNH\alpha} = \phi - 60°$ in the situations ±180°, –90°, ±0°, and +90°.

The coefficients C_0 signify mean J values obtained for a complete torsion-angle revolution, also referred to as *conformation averaged J* coupling constants. The differences ($C_2 - C_1$) are the largest deflections in J from the mean, where *primary* and *secondary* maxima of the curves at ±180° and ±0°, respectively, differ by $2C_1$.

Given sets of up to six ^3J parameters per torsion, the challenge is now to find that angle value in best agreement with the experimental data. Numerical methods exploiting the *redundance* present in large data pools permit the *self-consistent calibration* of Karplus coefficients during the course of the angle refinement (Schmidt et al., 1999). This obviates the need for traditional referencing of conformations derived from X-ray data.

We previously collected for flavodoxin values for the six possible coupling constants $^3J(\phi)$ and determined the protein's mainchain torsion angles ϕ (Schmidt et al., 1999). Discrepancy in ϕ between our NMR solution structure and comparison coordinates from X-ray crystallography (Walsh et al., 1998; Artali et al. 2002) is only 5° on average, which is smaller than the molecular dynamical angular libration due to thermal effects, indicating that both NMR solution and X-ray crystal structures of flavodoxin are very similar indeed.

Here, we record ^3J data for the enzyme Ribonuclease T1, a 104-residue protein (11 kDa) from *Aspergillus oryzae* (RNase T1, EC 3.1.27.3) that cleaves single-stranded RNA 3'-side of guanine nucleotides, and determine the majority of the ϕ torsion angles in the enzyme.

2. Materials and methods

One stringent requirement for efficient protein NMR analysis is that the protein sample be artifically enriched in the stable non-radioactive isotopes ^{15}N and ^{13}C, a process nowadays commonly applied in protein expression by recombinant technologies (Kainosho, 1997). Whilst oxygen does not play any role in protein NMR practice, the ^1H isotope offering greatest sensitivity is ubiquitous and abundant. Sometimes, it is being depleted by ^2H replacement in order to alleviate adverse signal relaxation effects occuring in large protein samples (above approximately 250 amino acids) exhibiting slow rotational tumbling rates (longer than approximately 10 ns rad^{-1}).

2.1 Protein sample

Uniformly ^{13}C,^{15}N-labeled RNase T1 (Lys25 isoenzyme) was obtained following established protocols (Quaas et al. 1988a,b; Spitzner et al., 2001) and used at 2-mM concentration in aqueous solution of pH 5.5 (containing 10% D_2O). All NMR spectra were recorded at 308 K. Prerequisite to any protein NMR analysis is the assignment of resonance signals to individual nuclei, not unlike a fingerprint of the molecule. Values quoted are chemical shifts in parts per million (ppm) from the respective ^1H, ^{13}C, or ^{15}N band base frequency. Resonance assignments for RNase T1 (Fig. 3) are available from the BioMagRes database for ^1H (BMRB-133; Hoffmann & Rüterjans, 1988) and for ^{15}N (BMRB-1658; Schmidt et al., 1991), and ^{13}C chemical shifts were given by Pfeiffer et al. (1996b). Comparison ϕ torsion angles were calculated from crystal coordinates, resolved at 0.15 nm, of RNase T1 complexed with Ca^{2+} (PDB-9RNT; Martinez-Oyanedel et al., 1991).

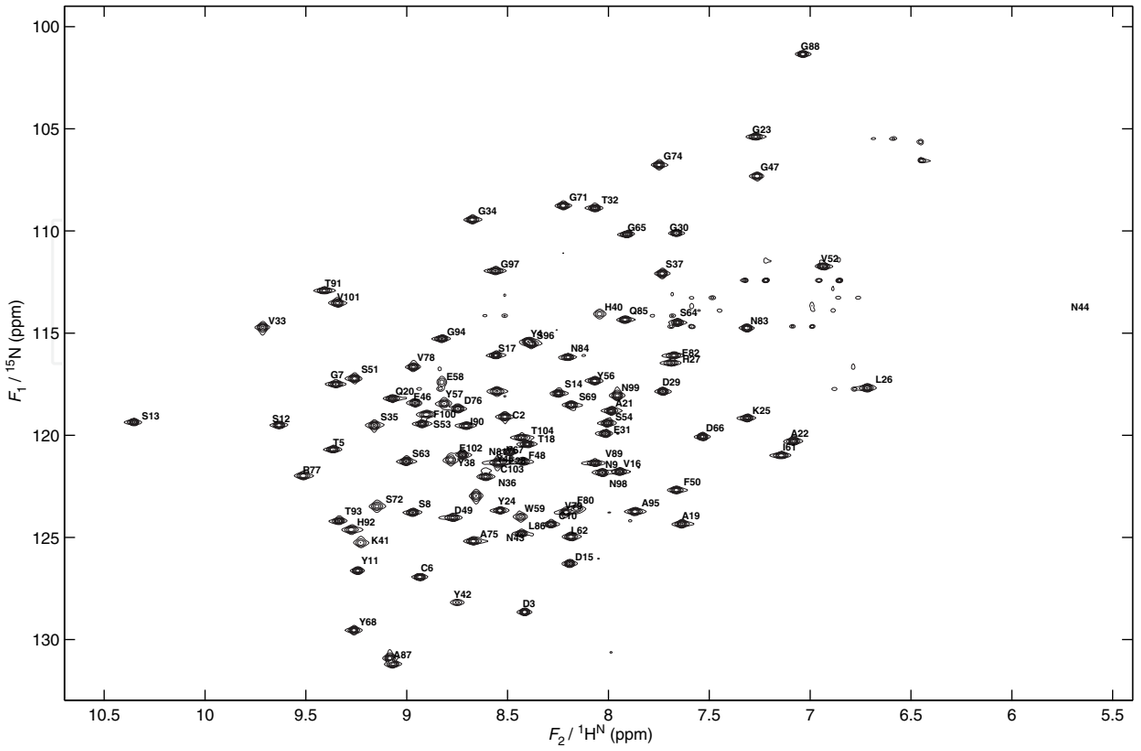

Fig. 3. ^{1}H,^{15}N-chemical shift correlation spectrum of RNase T1 at 900 MHz and 308 K.

2.2 Data collection

The focus of this chapter lies on protein structure and interpretation of NMR data. The reader interested in the details of NMR pulse-sequence design and the setup of multi-dimensional NMR experiments is referred to specialist textbooks (Roberts, 1993; Evans, 1995; Keeler, 2005; Hoch & Stern, 1996; Cavanagh et al., 2007) and to the literature including contained bibliography on the measurement of each of the six protein ϕ related ^3J coupling constants, as given in the separate NMR Experiments section at the end of the chapter.

Measurements of *J* coupling constants are subject to two principal concepts. One family of NMR experiments exploits *frequency modulation*, such as COSY, DQF-COSY, and E.COSY (Griesinger et al., 1987), giving rise to characteristic multiplet line splittings (Fig. 4). The other technique uses *amplitude modulation*, subdivided into *J*-modulation (Billeter et al., 1992) and *J*-correlation (Bax et al., 1994), encoding *J* in time-dependent signal intensity. Both approaches naturally have their pros and cons. While frequency-modulation schemes produce NMR signals of weaker intensity and larger space requirement, at times leading to signal overlap, amplitude-modulation schemes chiefly fail to measure small coupling constants.

To minimize signal overlap, protein NMR spectra are often recorded in 3D mode by exploiting the resonance of an auxiliary spin and selecting 2D projections at that frequency. Example graphs in Fig. 4 show such an experimental multiplet pattern, together with its best-fit least-squares lineshape reconstruction and the residual error signal.

2.3 Data evaluation

Whichever the chosen approach, the particular method applied to extract *J* values as structure parameters from NMR spectra must be considered an integral part of the analysis also. The authors gathered experience with both methods, albeit with an undeniable preference for E.COSY-type spectra which perform particularly robust in connection with computer-assisted lineshape analysis (Schmidt, 1997a; Löhr et al., 2000).

Contour plots of NMR signals for *J* analysis recorded in E.COSY mode show characteristic tilts (Griesinger et al., 1987), where a prominent large one-bond coupling spreads out the multiplet along the vertical spectrum dimension, so as to permit reading the sought smaller ^3J coupling off the frequency difference between the two multiplet halves in the horizontal dimension.

In the example of Fig. 4, the $^1J_{C\alpha H\alpha}$ of typically 143 Hz is exploited to split the signal into two halves along the F_1 dimension, given here by the $^{13}C^{\alpha}$ resonance frequency, and the small $^3J_{C'H\alpha}$ coupling results from the frequency difference between both halves along the perpendicular F_2 dimension, given here by the $^{13}C'$ carbonyl resonance.

The parameter record lists optimized values for coupling constants $^1J_{C\alpha H\alpha}$ and $^3J_{C'H\alpha}$ as the primary E.COSY components responsible for the tilted appearance of the signal shape in vertical and horizontal directions, respectively. Other parameters include, apart from amplitude scaling, line widths and line asymmetries in both dimensions, a second unresolved splitting pair.

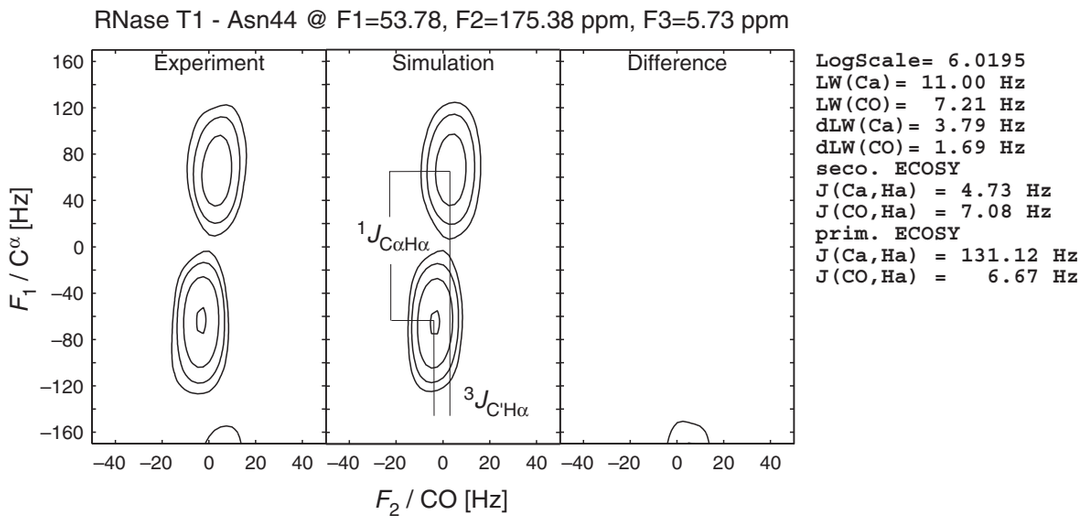

Fig. 4. Contour plot of a 500-MHz H(N)CA,CO[HA]-E.COSY multiplet recorded for RNase T1. Example analysis for extracting the $^3J_{C'H\alpha}$ coupling constant from the 2D $^{13}C^{\alpha}$,$^{13}C'$ correlation signal (F_1,F_2) taken at the resonance of the amide $^1H^N$ proton in the third dimension (F_3). The three nuclei eliciting the three spectrum dimensions all couple with the $^1H^{\alpha}$ spin (Fig. 1.), whose presence, following the E.COSY principle, is seen only as splittings, not as another frequency dimension.

3. Results

3.1 RNase T1

Using a uniformly ^{15}N and ^{13}C stable-isotope labeled sample of the enzyme RNase T1, a total 512 ^{3}J values were collected, related to the polypeptide mainchain torsion angles ϕ in 82 out of the total 104 amino-acid residues.

Even without fitting quantitative torsion angles to the ^{3}J data, qualitative inspection of the J values permits insights into some details of the protein's secondary structure already. For example, residue Asn44 in RNase T1 exhibits a very large $^{3}J_{C'H\alpha}$ coupling of 6.67 Hz (Fig. 4), second only to that seen in Asn84. This is irreconcilable with a ϕ torsion in the negative value range (Fig. 2). In addition, the $^{1}J_{C\alpha H\alpha}$ coupling of only 131 Hz (Fig. 4) falls well short of the expected average and supports a positive ϕ torsion, too. Consequently, Asn44 must exhibit a positive value for its ϕ torsion.

Signals for consecutive residues Asn43 and Asn44 in RNase T1 could hardly be more different. A value of 2.94 Hz for $^{3}J_{HNC\beta}$ in Asn43 (Fig. 5A) contrasts the lowly 0.47 Hz in Asn44 (Fig. 5B). Very different $^{1}J_{C\alpha C\beta}$ couplings also suggest differing backbone geometries. While the near-average $^{1}J_{C\alpha C\beta}$ coupling of 35.8 Hz in Asn43 is common with negative ϕ torsions, the unusually large 43.7-Hz coupling in Asn44 agrees better with a positive ϕ value (Schmidt et al., 2009). Both being asparagines, this cannot be a residue-type specific effect on the J couplings (Schmidt, 2007a).

The above-average value of 2.66 Hz seen for $^{3}J_{C'C\beta}$ in Tyr45 (Fig. 5C) is consistent with a type-I β turn spanning both Tyr45 and Glu46. This tyrosine's aromatic ring system is a critical component in nucleotide recognition and binding.

The consecutive residues Ala87 and Gly88 in RNase T1 form a β bulge (Chan et al., 1993). An unusually small $^{3}J_{HNC'}$ coupling near zero in Ala87 (Fig. 5D) and an unusually large 2.9-Hz $^{3}J_{C'C'}$ coupling in Gly88 (Fig. 5E) hint at ϕ torsion angles near +90°/–90° and 180° (Fig. 2), respectively, corroborating the distorted geometry in the central portion of a β strand.

Coupling type	Δϕ (deg)	C_0 (Hz)	C_1 (Hz)	C_2 (Hz)	*trans* J(180°) (Hz)	*gauche* J(±60°) (Hz)
$^{3}J_{HNH\alpha}$	–60°	5.67	–0.71	3.37	9.74	3.63
$^{3}J_{HNC'}$	180°	1.79	–0.75	1.56	4.09	0.64
$^{3}J_{HNC\beta}$	60°	2.32	–1.64	1.91	5.86	0.54
$^{3}J_{C'H\alpha}$	120°	3.21	–2.17	2.05	7.43	1.10
$^{3}J_{C'C'}$	0°	1.43	–0.96	0.76	3.15	0.58
$^{3}J_{C'C\beta}$	–120°	1.33	–0.51	0.91	2.75	0.62

Table 2. Karplus coefficients for Eq. 1, optimized against experimental ^{3}J data for RNase T1

A RNase T1 - Asn43 @ F1=62.71, F2=8.53 ppm, F3=125.32 ppm

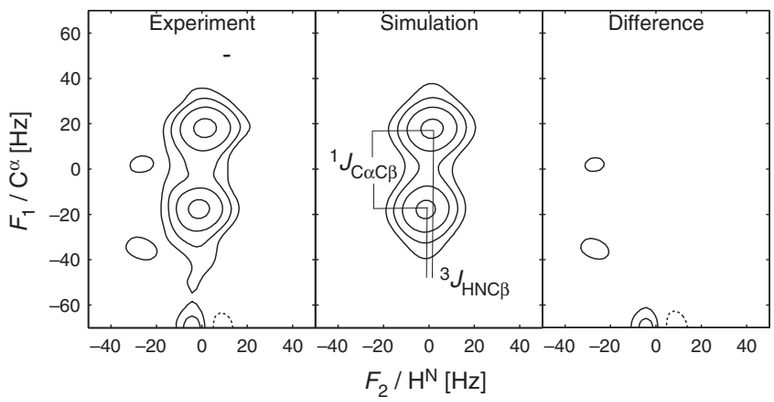


```
LogScale= 6.6491
LW(Ca)= 14.47 Hz
LW(HN)= 13.11 Hz
dLW(Ca)= 0.91 Hz
dLW(HN)= 0.75 Hz
seco. ECOSY
J(Ca,Cx) = 0.98 Hz
J(HN,Cx) = 6.29 Hz
prim. ECOSY
J(Ca,Cb) = 35.80 Hz
J(HN,Cb) =  2.94 Hz
```

B RNase T1 - Asn44 @ F1=61.82, F2=5.69 ppm, F3=113.92 ppm

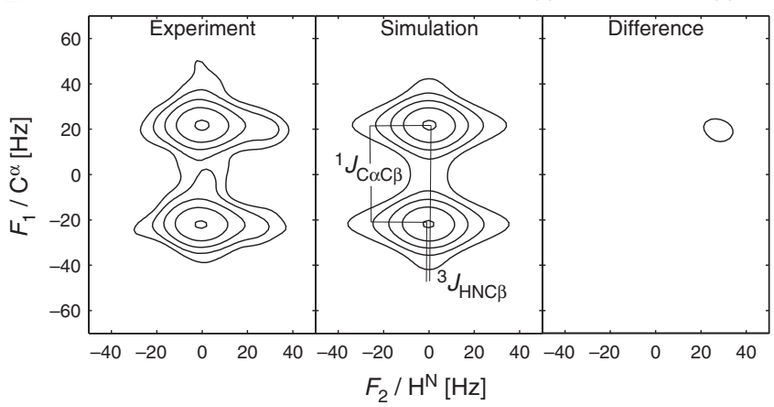


```
LogScale= 6.8681
LW(Ca)= 10.62 Hz
LW(HN)= 19.91 Hz
dLW(Ca)= 0.08 Hz
dLW(HN)= 0.41 Hz
seco. ECOSY
J(Ca,Cx) = 0.69 Hz
J(HN,Cx) = 3.62 Hz
prim. ECOSY
J(Ca,Cb) = 43.67 Hz
J(HN,Cb) =  0.47 Hz
```

C RNase T1 - Tyr45 @ F1=59.79, F2=177.47 ppm, F3=8.58 ppm

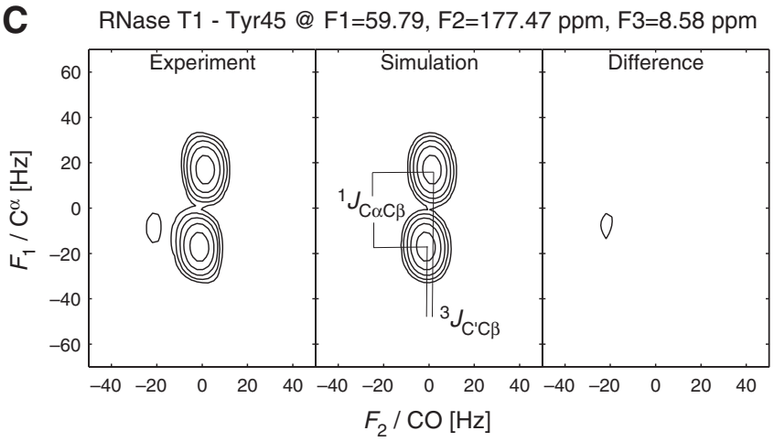


```
LogScale= 6.4622
LW(Ca)=  9.03 Hz
LW(CO)=  4.93 Hz
dLW(Ca)= 0.23 Hz
dLW(CO)= 0.10 Hz
seco. ECOSY
J(Ca,Cx) = 1.05 Hz
J(CO,Cx) = 3.46 Hz
prim. ECOSY
J(Ca,Cb) = 34.00 Hz
J(CO,Cb) =  2.66 Hz
```

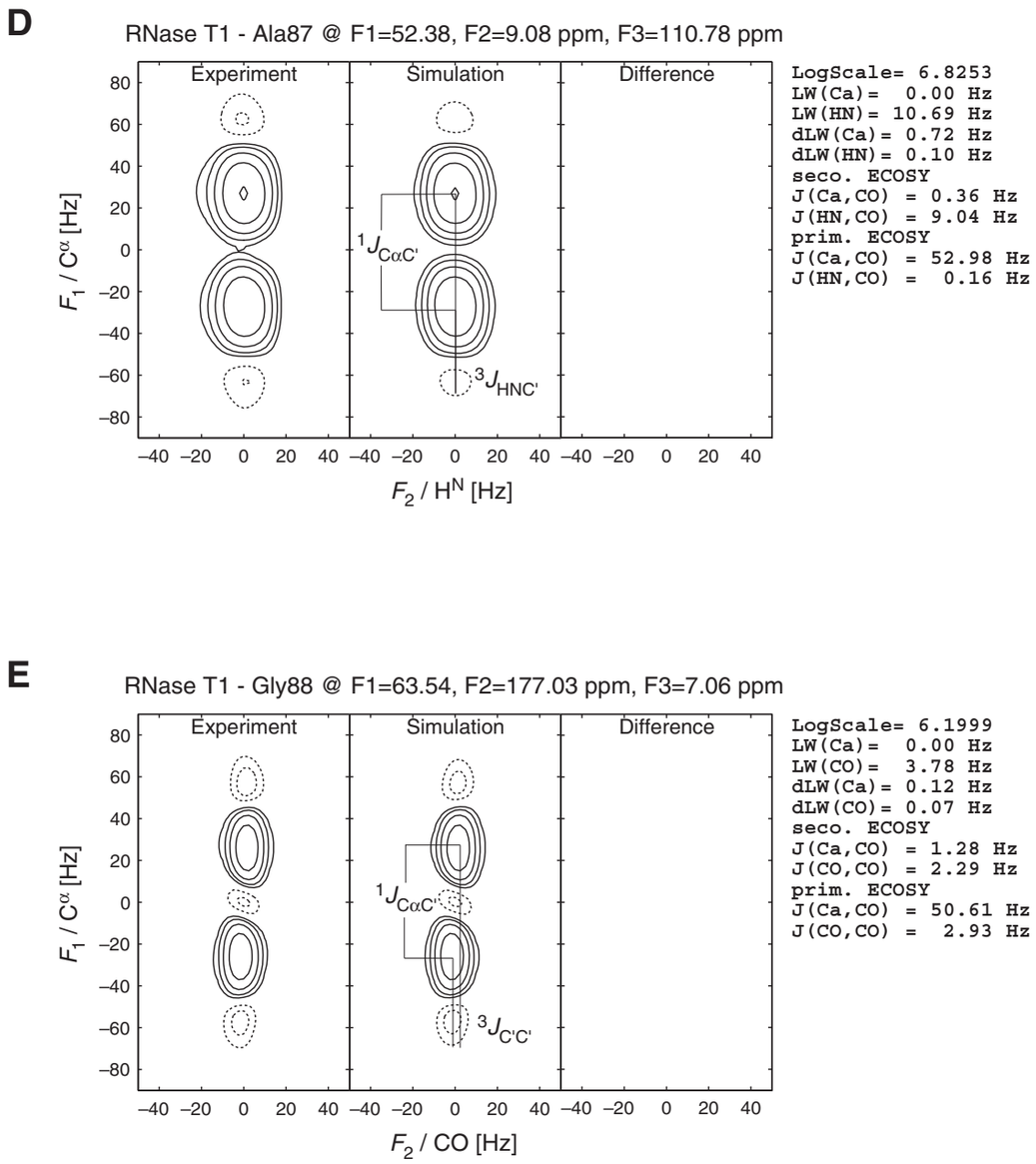

Fig. 5. Example 2D E.COSY multiplet sections from 3D NMR spectra recorded for RNase T1. *Panels A-C* (previous page): $^{3}J_{HNC\beta}$ and $^{3}J_{C'C\beta}$ evaluations exploiting the $^{1}J_{C\alpha C\beta}$ coupling of typically 35 Hz; *Panels D-E*: $^{3}J_{HNC'}$ and $^{3}J_{C'C'}$ evaluations exploiting the $^{1}J_{C\alpha C'}$ coupling of typically 53 Hz. Solid and dotted lines are positive and negative contours, respectively.

Eventually, the 82 ϕ torsion angles were fitted simultaneously to the pool of all 512 ^{3}J data. Self-consistently optimized in conjunction with the torsion-angle values, the Karplus curves shown in Fig. 6 and respective coefficients summarized in Table 2 represent the best fit to the ^{3}J data available for RNase T1 exclusively, yet, would be similar with other proteins also.

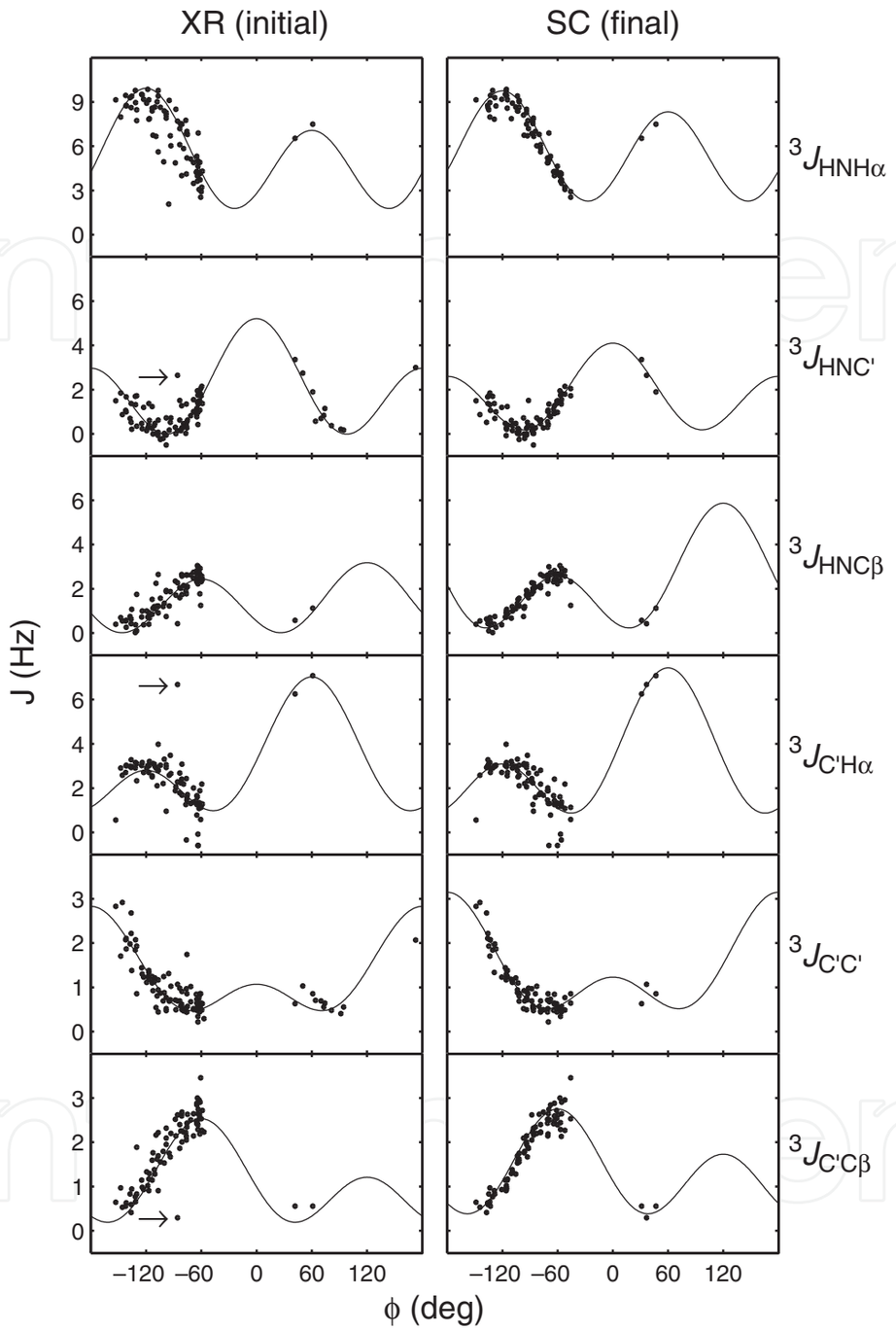

Fig. 6. Optimization of protein ϕ torsions on the basis of ^3J coupling constants. *XR panels*: Experimental data for RNase T1 (dots) plotted against initial torsion values calculated from crystal structure coordinates (PDB-9RNT). *SC panels*: The same data plotted against torsion values iteratively optimized by referring exclusively and simultaneously to all ^3J data, adjusting both torsion angles and Karplus coefficients in a self-consistent manner (Schmidt et al., 1999). Arrows point at Asn44 data that appear to be outliers initially.

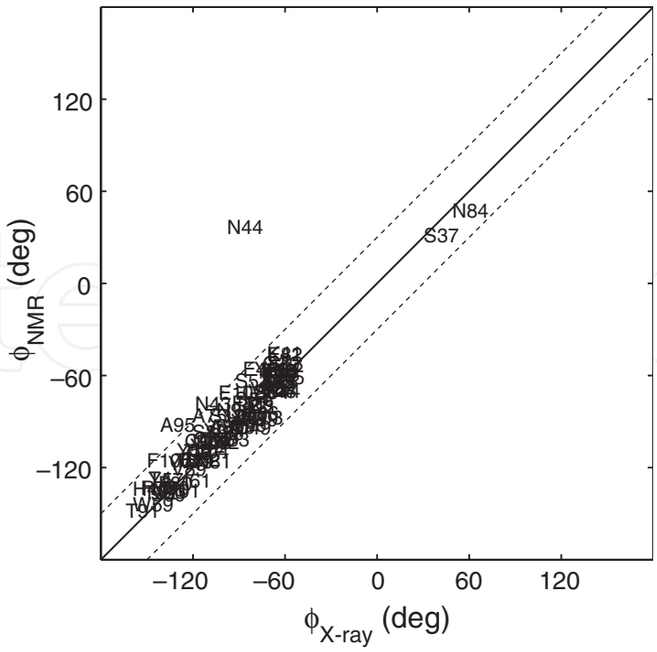

Fig. 7. Comparison of mainchain torsions ϕ in RNase T1 as inferred from self-consistent *J* coupling analysis and from crystallographic data (PDB-9RNT) by Martinez-Oyanedel et al. (1991). The majority of items agree within a tolerance of ±30° (dashed bounds). In the final optimized set, the Asn44 ϕ torsion angle has flipped from –86° to +37°.

Two facts rationalize the markedly reduced scatter seen in the right-hand-side $^3J_{HNH\alpha}$ panel in Fig. 6 compared with the other five coupling types: Firstly, being larger than $^3J_{HC}$ or $^3J_{CC}$ on an absolute scale, $^3J_{HH}$ values dominate the fit and, secondly, ϕ torsion values in regular protein structure typically fall on the steep slope of the $^3J_{HH}$ curve, making regression sensitive to small changes in $^3J_{HH}$. The residual scatter is due to unaccounted substituent effects in the different amino-acid types (Schmidt, 2007a), unaccounted torsion-angle dynamics (Brüschweiler & Case, 1994; Pérez et al., 2001), and random experimental error.

Assigned to Asn44 in RNase T1, the solitary data point in the left-hand-side $^3J_{C'H\alpha}(\phi)$ panel in Fig. 6, near the upper border, is elevated by around 3 Hz above the crowd. Apparently, other large $^3J_{C'H\alpha}$ coupling constants around 6-7 Hz connect with positive ϕ torsion angles. Contrasting the negative ϕ value found for Asn44 in crystal structure PDB-9RNT (Martinez-Oyanedel et al., 1991), the conformation in solution that emerged from our *J* coupling analysis differs from that in the solid state (Fig. 7). Similarity between relative *J* coupling values for Asn44 and those residues that exhibit positive ϕ angles clearly suggest that ϕ_{44} be rotated to a positive value also. Indeed, self-consistent optimization of ϕ torsions referencing the set of six ϕ-related coupling types converges at +37° for Asn44, while improving dramatically the error between observed coupling constants and those predicted from the crystal-structure angles.

The region around residues 42-48 of the enzyme engages in the recognition and binding of the substrate nucleotide (Fig. 8). Inspection of eight crystal structures of RNase T1 in a variety of complexes reveals that Asn44 adopts a negative ϕ value in only those structures

presenting a free binding site or, rather, a calcium, zinc, or vanadate metal ion bound to the *apo*-enzyme (9RNT, 8RNT, 3RNT). Similarly, the inadequate adenosine nucleotide complex (6RNT) also resembles the *apo*-enzyme. Even though the distant ribose phosphate interacts with catalytic residues His40 and Glu58 in this latter structure, the nucleobase is directed away from the enzyme, so as to leave the recognition loop unoccupied, for RNase T1 binding is G not A specific.

However, four other crystal structures of RNase T1 in various complexes, notably those with a bound guanine nucleotide (1RLS, 1RNT, 2RNT, 5RNT), do exhibit positive ϕ angles for Asn44 (Fig. 7). Also ϕ angles in the adjacent positions Asn43 and Tyr45 differ between the two groups, by approximately 40° and 10°, respectively.

The observations suggest that binding of the correct substrate elicits a concerted conformation change involving torsion ϕ_{44}, and likely ψ_{44}, too, as well as torsions ψ_{43} and ϕ_{45} in the preceding and subsequent residue, respectively. Yet, the NMR evidence tells a different story: Torsion angle ϕ_{44} is positive already in our sample of the free enzyme in aqueous solution that was subjected to NMR measurement! Conformational variability of the Asn44 backbone, such as continual flips between positive and negative values, can be ruled out on the basis of the large $^3J_{C'H\alpha}$ coupling value observed, as such conformational averaging would reduce the *J* value towards its mean of about half the size (Table 2).

A likely explanation for the negative angle value in some of the crystal structures would be packing effects through molecules in adjacent grid cells distorting the conformation of the rather exposed 42-48 loop region at the protein surface. Another possible explanation could be that the metal agents added to aid the crystallization process obstruct the binding site differently than the natural substrate would do.

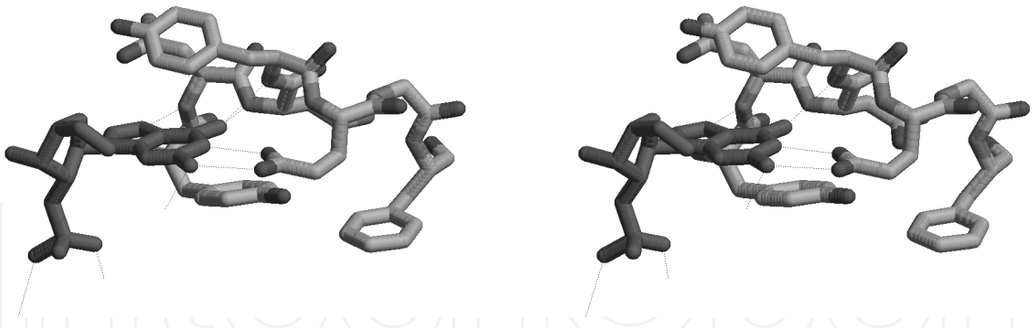

Fig. 8. Stereo view of residues 42-48 in the crystal structure of the RNase T1:2′GMP inhibitor complex (PDB-1RNT, Arni et al., 1988). Involved in nucleotide recognition and binding, Asn43 and Asn44 backbone amide groups interact with the guanine five- and six-ring, respectively, while the Glu46 sidechain carboxylate probes the presence of the correct hydrogen bonding capacity at the Watson-Crick edge of the guanine. Tyr42 and Tyr45 sandwich the guanine ring plane.

3.2 Flavodoxin

^3J coupling data from a similar study targeting backbone torsion angles ψ in flavodoxin suggested subtle differences between the structures of this protein in aqueous solution

(NMR) and in the crystalline solid state (X-ray). For example, on the basis of *J* coupling constants the orientation of peptide plane Ala39/Ser40 shown in the X-ray structure needed to be adjusted by about +10° in order to fulfil the experimental data (Löhr et al., 2001).

A conformational hot spot is found in flavodoxin's so-called "60-loop", the region protruding around the isoalloxazine ring system, made up of Gly61-Asp62-Asp63-Ser64. Results from our analysis on the exclusive basis of *J*-coupling constants agree with what has been known for some time already from X-ray studies on flavodoxin (Watenpaugh et al., 1976). These crystal structures of flavodoxin can be grouped according to 2FX2, 3FX2, 1J8Q, and 'WFX2'[1], on one side, and 4FX2, 5FX2, 1BU5A, and 1BU5B, on the other. The former group represents oxidized species of the FMN cofactor, the latter includes reduced (5FX2) and semi-reduced (4FX2) quinone forms. 1BU5A and 1BU5B (Walsh et al., 1998) are two chains in an asymmetric unit of *apo*-flavodoxin-riboflavin complex lacking the ribose phosphate.

Conformations of torsions ψ_{61} and ϕ_{62} in flavodoxin differ by almost 180° between both structure sets, implying a flip of the intervening peptide plane with connected changes in the hydrogen bonding network. Our NMR data on the oxidized species support the torsion angles derived from the first group. Most notably, Asp62 adopts a rare positive ϕ torsion angle responsible for an elevated $^3J_{C'H\alpha}$ coupling constant of 5.1 Hz. As it is also connected with an unusual negative ψ torsion, this data point stands out in a graph of $^3J_{C'H\alpha}(\psi)$ (not shown). Albeit a non-glycine residue, Asp62 exhibits a secondary-structure feature normally characteristic of glycine as frequently found in a type-II' β turn motif (Creighton, 1993). But then, the surrounding torsion angles are too distorted to form a proper reverse turn. Variability in this loop region is also corroborated by an analysis of coupling constants related to the sidechain χ_1 torsion angle (Schmidt, 2007b).

4. Discussion, conclusion and scope

Complete determination of a protein fold from scratch is inherently impossible on the sole basis of *J* coupling restraints alone, owing to their short-range nature of interaction. Even though ϕ torsion angles can be determined fairly accurately, and values of ψ can at least be narrowed to plausible ranges, while fixing ω torsions at the planar 180° value, the chaining of the distinct amino-acid fragments is likely to cause errors to accumulate in the process. A few long-range restraints, such as those provided by the measurement of NOE effects, will normally be required to ensure the correct fold over the whole polypeptide chain. In fact, the present results derived from our *J*-coupling data are consistent with an independent previous investigation into the RNase T1 solution structure by means of the traditional measurement of NOE effects that were subsequently converted into proton-proton distance constraints (Pfeiffer et al., 1996a).

4.1 Data correlation and redundancy

The ϕ torsion angle in each amino-acid residue is supported by up to six ^3J coupling constants, which, in aggregate, determine just one internal rotational degree of freedom of the molecular model, the value of ϕ. Even though the *J* data are all independent

[1] 'WFX2' signifies a preliminary X-ray coordinate set of *D. vulgaris* flavodoxin not available from the PDB and kindly provided by Martin Walsh, University College Galway, Ireland.

observations, they do not represent six independent structure parameters. Owing to their simultaneous dependence on the same torsion, their values are highly correlated, or anti-correlated, for that matter (Table 3). Somewhat limited by pairs of couplings exhibiting correlated angle dependence (Fig 2), the amount of independent structure information available reduces to effectively 3 or 4, rather than 6, yet still exceeds the single rotational degree sought to be fixed. Precisely this redundance, however, is key to determining torsion angles accurately.

	$^3J_{HNH\alpha}$	$^3J_{HNC'}$	$^3J_{HNC\beta}$	$^3J_{C'H\alpha}$	$^3J_{C'C'}$	$^3J_{C'C\beta}$
$^3J_{HNH\alpha}$	6.77 ± 2.12	–0.82	–1.20	1.18	0.81	–1.13
$^3J_{HNC'}$	–44%	0.89 ± 0.74	–0.11	0.27	0.27	–0.19
$^3J_{HNC\beta}$	–79%	–2%	1.62 ± 0.85	–0.82	–0.62	0.77
$^3J_{C'H\alpha}$	54%	8%	–61%	2.32 ± 1.29	0.47	–0.84
$^3J_{C'C'}$	58%	16%	–76%	30%	0.97 ± 0.58	–0.59
$^3J_{C'C\beta}$	–79%	–6%	89%	–69%	–77%	1.83 ± 0.78

Table 3.Variance-covariance matrix for 512 ϕ-related ^3J coupling constants in RNase T1[2]

4.2 Molecular dynamics effects

At times, the excess information contained in a set of observables can give insights into dynamic effects that may prevail in the molecular structure (Schmidt, 1997b). Conformational dynamics frequently complicate the analysis of amino-acid sidechain torsion angles χ_1 and need be taken into account for satisfactory interpretation of experimental J data related to that angle type. A variety of angular-mobility models can be applied to cases in which a single fixed torsion does not explain the observed data satisfactorily. Analyses commonly assume the χ_1 torsion either to dwell preferentially in energetically favourable staggered states (Pachler, 1963, 1964; Hansen et al., 1975) or to librate about a mean value according to a Gaussian probability profile (Jardetzky, 1980; Karimi-Nejad et al., 1994; Brüschweiler & Case, 1994).

In the first approach, amino-acid sidechain torsions are analyzed assuming the presence of interconverting staggered-rotamer conformations of χ_1 = –60°, ±180° and +60° to solve for the respective populations, p_1, p_2, and p_3, by linear combinations of so-called *trans* and *gauche* coupling values (Table 2). The Gaussian model, however, typically limits the torsion to one predominant conformation, yet, allowing for larger angular variability, at times. To this end, angular standard deviations of approximately 60° can be considered to represent a fully revolving torsion. Both models are somewhat complementary, the staggered-rotamer one being easier to apply, whereas the Gaussian one usually fits the data better (Schmidt, 1997b).

[2] Diagonal: mean and standard deviation (square-root of variance, in Hz). Upper triangle: standard deviation attributed to joint variation in both J types (square-root of covariance, in Hz), negative signs indicating antivariance. Lower triangle: pair-correlation coefficients.

4.3 ^1J and ^2J couplings in protein structure analysis

Interest is arising in short-range ^1J and ^2J coupling constants (Wienk et al., 2003; Löhr et al., 2011) as these are comparatively easier to measure than ^3J, albeit less well understood regarding their conformational dependence (Schmidt et al., 2009, 2010). However, by simply recognizing qualitative classes of small, medium, and large magnitudes for the respective parameters, it was feasible to pinpoint the boundaries of secondary-structure elements in a protein (Schmidt et al., 2011). The suggested procedure of *J*-indexing also exploits data redundance as each torsion angle is surrounded by large numbers of ^1J and ^2J coupling constants (Fig. 9).

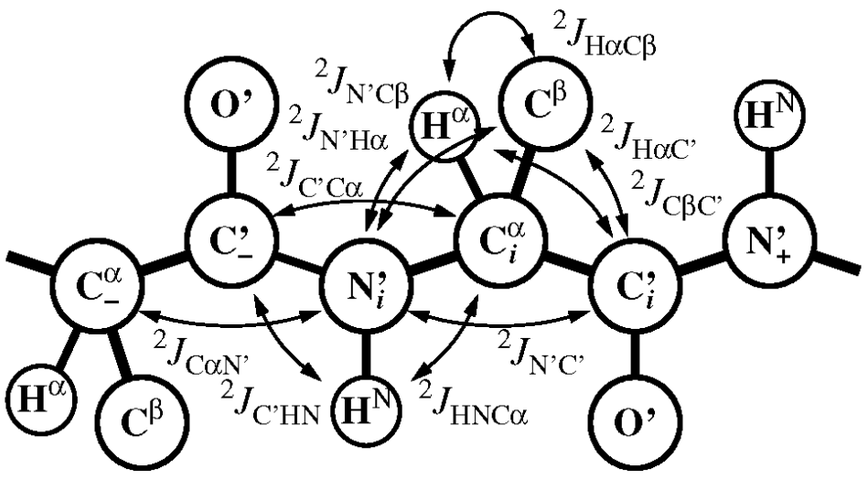

Fig. 9. The ten types of ^2J coupling constants encountered in the protein backbone.

Protein ^1J-, ^2J-, and ^3J-coupling constant data related to one-, two-, and three-bond interaction, respectively, continue being deposited by NMR spectroscopists with the Biological Magnetic Resonance Data Bank (BMRB, Ulrich et al., 2008) (Fig. 10).

4.4 Accuracy issues

Quantitative ^3J-coupling analysis in proteins appears to have reached a level of detail and accuracy at which a change of a few degrees in a torsion angle, comparable to thermal librational amplitudes, makes a noticeable difference, allowing, for example, genuine differences between NMR-based solution and X-ray based crystal structures to be detected.

The process of defining useful conformational constraints on the basis of *J* coupling constants usually requires, first, extracting accurate values for the *spin-system* related property *J* from NMR spectra and, second, translating these values into *molecular-geometry* related dihedral-angle values within the framework of a specified model of molecular structure and possibly dynamics. Naturally, both these stages come with their inherent inaccuracies which will impact on the final result (Fig. 11).

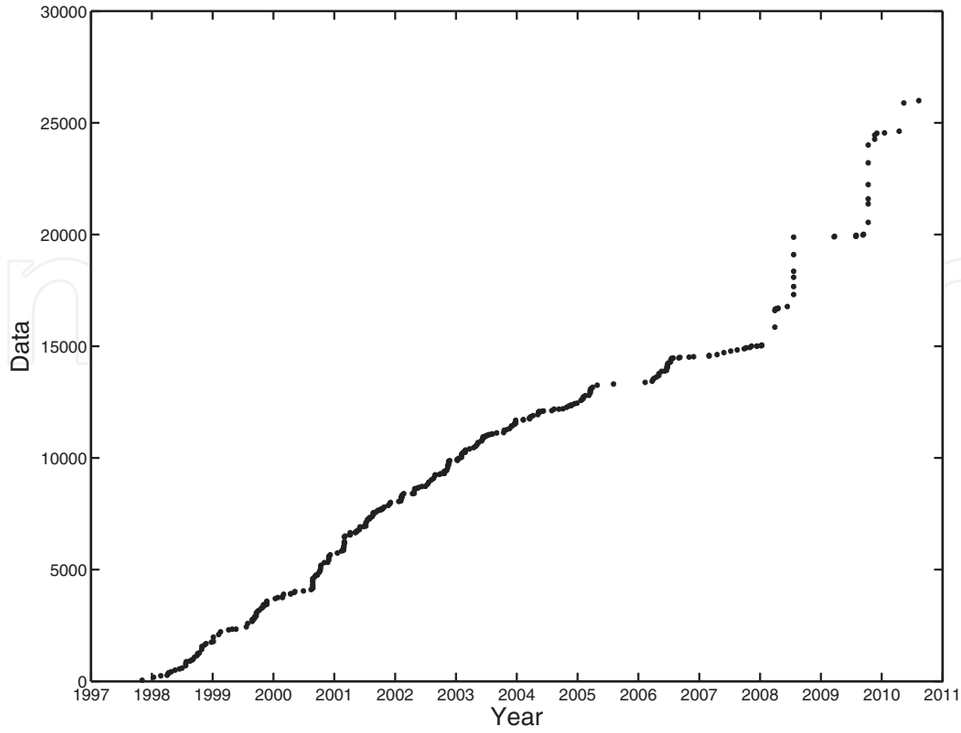

Fig. 10. Cumulative data volume submitted to the BMRB in category protein *J* coupling constants. The current number of deposited sets is around 350, totaling more than 25,000 values, the majority of which are $^{3}J_{HNH\alpha}$ coupling constants. Recent leaps reflect large-scale depositions of hitherto less popular ^{1}J and ^{2}J parameters which the authors of this chapter have set out to explore regarding utility in protein structure determination (Schmidt et al., 2009, 2010).

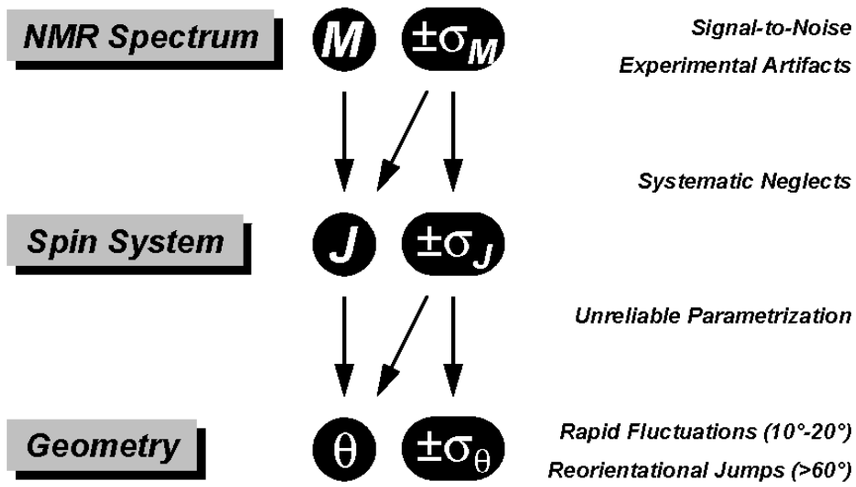

Fig. 11. Progression of procedural errors and random uncertainties into molecular structure.

A word of caution is advised though. Even if both above mentioned evaluation stages as well as the recording of NMR spectra were void of systematic error, i.e., not limited by their technical approach, molecules don't always do us the favour of revealing an unambiguous structure. If conformational dynamics are at play, such ambiguity is not to be confused with lack of accuracy or precision, and the geometry of the molecule must not be squeezed into a 'strait-jacket', as it were. Rather we need to develop our understanding of molecular structure, if not re-define the term, in a way that integrates both dynamic as well as static aspects of conformation. Research into partially or intrinsically disordered protein structures is witness to such development (Dyson & Wright, 1998).

5. NMR Experiments

J coupling measurements were carried out on NMR spectrometers manufactured by Bruker, Rheinstetten, Germany, with nominal fields ranging from 500 to 900 MHz proton frequency. All instruments were fitted with cryogenically cooled triple-resonance z-axis pulsed-field-gradient probes, except the 500-MHz instruments were equipped with room-temperature triple-resonance three-axis pulsed-field-gradient probes.

Experiment names of the exclusive correlation spectroscopy (E.COSY) follow a convention that identifies by uppercase lettering those protein nuclei that are active in generating the spectrum dimensions, in round parentheses those used for magnetization relay only, and in square brackets the presence of those passive spins that give rise to the sought *J* coupling interaction (Wang & Bax, 1995).

Each coupling constant was measured at least twice, and mean values quoted carry two standard deviations, the former denoting the *intra*-spectrum, i.e., variation across all amino-acid residues, and the latter denoting the standard error or *inter*-spectrum rms variation between the repeat experiments, i.e., a measure of reproducibility.

5.1 $^3J(H^N,H^\alpha)$ coupling constants

$^3J_{HNH\alpha}$ coupling constants originated from 3D-HA[HB,HN](CACO)NH quantitative *J* correlation spectra recorded at 500 MHz (Löhr et al., 1999). The coupling constant for residue i was evaluated in spectrum planes at the resonance N_{i+1} by summing the data points comprising the H^N_i,H^N_{i+1} cross peak and referring its intensity to the H^α_i,H^N_{i+1} auto peak according to $I_{cross}/I_{auto} = -\tan^2(\pi J\Delta)$, with the magnetization-transfer delay, Δ, set at 17 ms. Raw coupling constants were corrected for H/D exchange by an average factor of 1.049, due to scaling all I_{cross}/I_{auto} ratios for the 10-% D_2O solvent component needed for field-frequency locking. Both datasets yielded 77 values of corrected $^3J_{HNH\alpha}$ averaging 6.77 ± 2.17 ± 0.24 Hz.

5.2 $^3J(H^N,C')$ coupling constants

$^3J_{HNC'}$ coupling constants were determined by least-squares fitting 2D projections of E.COSY-type C^α,H^N multiplets (Schmidt et al., 1997a) recorded at 900 MHz using a [^{15}N,^{1}H]-TROSY variant (Pervushin et al., 2000) of 3D-(H)CANNH[CO] spectra (Löhr & Rüterjans, 1995). To minimize transverse relaxation effects during the constant-time period, C^α

chemical shifts and $^1J_{C\alpha C'}$ couplings were simultaneously evolved in a $^1H^\alpha$,$^{13}C^\alpha$ multiple-quantum constant-time t_1 period while spin-locking $^1H^\alpha$ magnetization using a 3-kHz spin-lock field. Insufficient to cover the complete H^α shift range uniformly, poorly decoupled C^α resonances near the excitation band edges were omitted from evaluation. Glycine patterns were disregarded entirely as the NMR experiment is not optimized for their twin-H^α spin topology. The highly reproducible results comprised 70 values of $^3J_{HNC'}$ averaging 0.75 ± 0.71 ± 0.06 Hz. For many of those residues that needed to be ignored in (H)CANNH evaluations for reasons of lineshape distortion or overlap, $^3J_{HNC'}$ coupling constants were obtained using a simpler 3D-heteronuclear relayed-E.COSY approach at 500 MHz in combination with more sophisticated antiphase 2D-multiplet line-shape analysis (Schmidt et al., 1996). The 76 values averaged 0.86 ± 0.72 ± 0.17 Hz, slightly larger than those from (H)CANNH. Additional values were extracted from a [^{15}N,^{1}H]-TROSY version of ct-HNCA[CO]-E.COSY spectra (Wang & Bax, 1995) recorded at 600 MHz, averaging 0.81 ± 0.79 ± 0.21 Hz and bringing the total number of items to 92, including data for glycine. Rmsd between all six spectra was 0.22 Hz.

5.3 $^3J(H^N,C^\beta)$ coupling constants

$^3J_{HNC\beta}$ coupling constants were determined by simulating 2D projections of C^α,H^N multiplets resulting from a [^{15}N,^{1}H]-TROSY version of the 3D-HNCA[CB]-E.COSY experiment (Wang & Bax, 1996) carried out at 800 MHz. Glycines generally lacking the C^β nucleus were ignored. Overlapping C^α_i and C^α_{i-1} resonances prevented a few coupling constants from being obtained. Coincident C^α and C^β chemical-shift ranges in serine and threonine residues precluded selective excitation of either nucleus and respective data were disregarded. Thus, the two recordings yielded only 58 values, averaging 1.50 ± 0.94 ± 0.09 Hz. Additional $^3J_{HNC\beta}$ coupling constants resulted however from 3D [^{15}N,^{1}H]-TROSY-HNCB quantitative *J* correlation experiments (F. Löhr, unpublished) performed at 600 and 800 MHz. Dephasing of $^1H^N$ coherence due to passive $^3J_{HNH\alpha}$ couplings during *J* evolution delay Δ, which was set at either 40 or 45 ms, was avoided by employing BIRD refocusing elements (Garbow et al., 1982) in the centre of the Δ period. Three spectra yielded 68 values of $^3J_{HNC\beta}$ averaging 1.71 ± 0.79 ± 0.18 Hz between quantitative *J* correlation data. Between all five sets, 81 values were determined at 1.62 ± 0.85 ± 0.14 Hz.

5.4 $^3J(C'_{i-1},H^\alpha_i)$ coupling constants

$^3J_{C'H\alpha}$ coupling constants resulted from fitting 2D projections of C^α_i,C'_{i-1} multiplets in 3D-H(N)CA,CO[HA]-E.COSY spectra (Löhr & Rüterjans, 1997; Löhr et al., 1997) recorded at 500 MHz. The total 81 values collected averaged 2.33 ± 1.29 ± 0.16 Hz.

5.5 $^3J(C'_{i-1},C'_i)$ coupling constants

$^3J_{C'C'}$ coupling constants resulted from fitting 2D projections of C^α_i,C'_{i-1} multiplets in 3D-H(N)CA,CO[CO]-E.COSY spectra (Löhr et al., 1997) recorded at 500 MHz. Glycine couplings included, the two datasets comprised 90 $^3J_{C'C'}$ values averaging 0.84 ± 0.65 ± 0.16 Hz. Additional $^3J_{C'C'}$ coupling constants resulted from quantitative *J*-correlation experiments

using a [^{15}N,^{1}H]-TROSY version of the 3D HN(CO)CO pulse sequence (Hu & Bax, 1996). Two spectra were acquired at 500 MHz with the *J*-evolution period Δ set at either 50 or 60 ms. The spectra allowed both sequential coupling constants $^{3}J(C'_{i-2},C'_{i-1})$ and $^{3}J(C'_{i-1},C'_{i})$ to be evaluated, yielding 78 values averaging 1.03 ± 0.61 ± 0.23 Hz. The final set comprised 98 coupling constants of 0.95 ± 0.63 ± 0.26 Hz.

5.6 $^{3}J(C'_{i-1},C^{\beta}_{i})$ coupling constants

$^{3}J_{C'C\beta}$ coupling constants were measured at 500 MHz by H(N)CA,CO[CB]-E.COSY (Löhr et al., 1997), yielding only 59 values averaging 1.96 ± 0.86 ± 0.16 Hz. As with $^{3}J_{HNC\beta}$, determining $^{3}J_{C'C\beta}$ coupling constants with these E.COSY-type experiments fails for serine, threonine, and some leucine residues, all exhibiting downfield-shifted $^{13}C^{\beta}$ resonances, so as to overlap with C^{α} chemical-shift ranges, preventing selective excitation. In contrast, HN(CO)CB quantitative *J* correlation (Hu & Bax, 1997) provides values for all residue types as long as the active coupling magnitude exceeds a certain threshold determined primarily by the signal-to-noise ratio. Spectra were acquired at 500 MHz with delays Δ set at either 37.5 or 38.5 ms to match $2/^{1}J(C',C^{\alpha})$. The ^{13}C carrier frequency was positioned at either 26 or 60 ppm. Quantitative *J* correlation yielded 74 data, averaging 1.83 ± 0.75 ± 0.10 Hz. Additional $^{3}J_{C'C\beta}$ values including those in Ser and Thr residues were obtained from C^{α}_{i},C'_{i-1} multiplet projections in H(N)CO,CA[CA]-E.COSY recorded at 800 MHz (F. Löhr, unpublished). The 76 values averaged 1.66 ± 0.80 ± 0.20 Hz, and the grand average over all ten sets was 1.82 ± 0.78 ± 0.20 Hz, totaling 82 values.

6. Supplementary material

^{3}J coupling constants related to the ϕ-torsion angles in RNase T1 as determined in the present work are deposited with the BioMagRes Database (accession number BMRB-16469), available at http://www.bmrb.wisc.edu/cgi-bin/explore.cgi?format=raw&bmrbId=16469

7. Acknowledgements

Norman Spitzner (Frankfurt university) is thanked for preparing a doubly-labelled RNase T1 sample. Robert Pritchard (graduate from Kent university) is thanked for helping evaluate RNase T1 spectra in the course of his undergraduate final-year project. Financial support by the Access to Research Infrastructures activity in the 7th Framework Programme of the EC (Project number: 261863, Bio-NMR) is gratefully acknowledged.

8. References

Arni, R., Heinemann, U., Maslowska, M., Tokuoda, R. & Saenger, W. (1988) Restrained least-squares refinement of the crystal structure of the ribonuclease T1*2'-guanylic acid complex at 1.9 Å resolution. *Acta Crystallographica Section B*, Vol. 43, pp. 534-554, ISSN 0108-7681 (p) 1600-5740 (e)

Artali, R., Bombieri, G., Meneghetti, F., Gilardi, G., Sadeghi, S.J., Cavazzini, D. & Rossi, G.L. (2002) Comparison of the refined crystal structure of wild-type (1.34 Å) flavodoxin from *Desulfovibrio vulgaris* and the S35C mutant (1.44 Å) at 100 K. *Acta Crystallographica Section D*, Vol. 58, pp. 1787-1792, ISSN 0907-4449 (p) 1399-0047 (e)

Bax, A., Vuister, G.W., Grzesiek, S., Delaglio, F., Wang, A.C., Tschudin, R. & Zhu, G. (1994) Measurement of homo- and heteronuclear J couplings from quantitative J correlation. Methods in Enzymology, Vol. 239, pp. 79-105, ISBN 0-12-182140-4

Billeter, M., Neri, D., Otting, G., Qian, Y.Q. & Wüthrich, K. (1992) Precise vicinal coupling constants $^{3}J_{HN\alpha}$ from nonlinear fits of *J*-modulated [^{15}N,^{1}H]-COSY-experiments. *Journal of Biomolecular NMR*, Vol. 2, pp. 257-274, ISSN 0925-2738 (p) 1573-5001 (e)

Blümel, M., Schmidt, J.M., Löhr, F. & Rüterjans, H. (1998) Quantitative ϕ torsion angle analysis in *Desulfovibrio vulgaris* flavodoxin based on six ϕ related ^{3}J couplings. *European Biophysics Journal*, Vol. 27, pp. 321-334, ISSN 0175-7571 (p) 1432-1017 (e)

Brüschweiler, R. & Case, D.A. (1994) Adding harmonic motion to the Karplus relation for spin-spin coupling. *Journal of the American Chemical Society*, Vol. 116, pp. 11199-11200, ISSN 0002-7863 (p) 1520-5126 (e)

Bystrov, V.F. (1976) Spin-spin coupling and the conformational states of peptide systems. *Progress in NMR Spectroscopy*, Vol. 10, pp. 41-81, ISSN 0079-6565

Cavanagh, J., Fairbrother, W.J., Palmer III, A.G., Rance, M. & Skelton, N.J. (2007) *Protein NMR spectroscopy: principles and practice*, Academic Press, San Diego, California, ISBN 978-0-12-164491-8 / 0-12-164491-X

Chan, A.W.E., Hutchinson, E.G. & Harris, D. (1993) Identification, classification, and analysis of beta-bulges in proteins. *Protein Science*, Vol. 2, 1574-1590, ISSN 0961-8368 (p) 1469-896x (e)

Creighton, T.E. (1993) *Proteins: structures and molecular properties*, 2nd ed., W. H. Freeman and Co., New York, ISBN 0-7167-7030-X

Dyson, H.J. & Wright, P.E. (1998) Equilibrium NMR studies of unfolded and partially folded proteins. *Nature Structural Biology*, *Supplement*, Vol. 5, pp. 499-503, ISSN 1072-8368

Ejchart, A. (1999) Scalar couplings in structure determination of proteins. *Bulletin of the Polish Academy of Sciences-Chemistry*, Vol. 47, pp. 1-19, ISSN 0239-7285

Engh, R.A. & Huber, R. (1991) Accurate bond and angle parameters for X-ray protein structure refinement. *Acta Crystallographica Section A*, Vol. 47, pp. 392-400, ISSN 0108-7673 (p) 1600-5724 (e)

Engh, R.A. & Huber, R. (2006) Structure quality and target parameters in *International Tables for Crystallography* Vol. F, Chapter 18.3, pp. 382–392, ISBN 978-1-4020-4969-9

Ernst, R.R., Bodenhausen, G. & Wokaun, A. (1987) *Principles of nuclear magnetic resonance in one and two dimensions*, Oxford University Press, Oxford, ISBN 0-19-855629-2

Evans, J.N.S. (1995) *Biomolecular NMR spectroscopy*, Oxford University Press, Oxford, ISBN 0-19-854766-8

Fischer, M.W.F., Losonczi, J.A., Weaver, J.L. & Prestegard, J.H. (1999) Domain orientation and dynamics in multidomain proteins from residual dipolar couplings. *Biochemistry*, Vol. 38, pp. 9013-9022, ISSN 0006-2960 (p) 1520-4995 (e)

Garbow, J.R., Weitekamp, D.P. & Pines, A. (1982) Bilinear rotation decoupling of homonuclear scalar interactions. *Chemical Physics Letters*, Vol. 93, pp. 504-509, ISSN 0009-2614

Griesinger, C., Sørensen, O.W. & Ernst, R.R. (1987) Practical aspects of the E. COSY technique. Measurement of scalar spin-spin coupling constants in peptides. *Journal of Magnetic Resonance*, Vol. 75, pp. 474-492, ISSN 0022-2364

Hansen, P.E., Feeney, J. & Roberts, G.C.K. (1975) Long range ^{13}C-^{1}H spin-spin coupling constants in amino acids. Conformational applications. *Journal of Magnetic Resonance*, Vol. 17, pp. 249-261, ISSN 0022-2364

Hennig, M., Bermel, W., Schwalbe, H. & Griesinger, C. (2000) Determination of ψ torsion angle restraints from $^{3}J(C_{\alpha},C_{\alpha})$ and $^{3}J(C_{\alpha},H_{N})$ coupling constants in proteins. *Journal of the American Chemical Society*, Vol. 122, pp. 6268–6277, ISSN 0002-7863 (p) 1520-5126 (e)

Hoch, J.C. & Stern, A.S. (1996) *NMR data processing*, John Wiley and Sons, New York, ISBN 978-0-471-03900-6

Hoffmann, E. & Rüterjans, H. (1988) Two-dimensional ^{1}H-NMR investigation of ribonuclease T1. *European Journal of Biochemistry*, Vol. 177, pp. 539-560, ISSN 0014-2956 (p) 1432-1033 (e)

Hu, J.-S. & Bax, A. (1996) Measurement of three-bond ^{13}C-^{13}C *J* couplings between carbonyl and carbonyl/ carboxyl carbons in isotopically enriched proteins. *Journal of the American Chemical Society*, Vol. 118, pp. 8170-8171, ISSN 0002-7863 (p) 1520-5126 (e)

Hu, J.-S. & Bax, A. (1997) Determination of ϕ and χ^{1} angles in proteins from ^{13}C-^{13}C three-bond couplings measured by three-dimensional heteronuclear NMR. How planar is the peptide bond? *Journal of the American Chemical Society*, Vol. 119, pp. 6360-6368, ISSN 0002-7863 (p) 1520-5126 (e)

IUPAC-IUB Commision on Biochemical Nomenclature (1970) Abbreviations and symbols for the description of the conformation of poplypeptide chains. Tentative rules (1969). *Biochemistry*, Vol. 9, pp. 3471-3479, ISSN 0006-2960

Jardetzky, O. (1980) On the nature of molecular conformations inferred from high-resolution NMR. *Biochimica et Biophysica Acta*, Vol. 621, pp. 227-232, ISSN 0006-3002

Kainosho, M. (1997) Isotope labelling of macromolecules for structural determinations. *Nature Structural Biology*, Vol. 4, Suppl. S, pp. 858-861, ISSN 1072-8368

Karimi-Nejad, Y., Schmidt, J.M., Rüterjans, H., Schwalbe, H. & Griesinger, C. (1994) Conformation of valine side chains in ribonuclease T1 determined by NMR studies of homonuclear and heteronuclear ^{3}J coupling constants. *Biochemistry*, Vol. 33, pp. 5481-5492, ISSN 0006-2960 (p) 1520-4995 (e)

Karplus, M. (1963) Vicinal proton coupling in nuclear magnetic resonance. *Journal of the American Chemical Society*, Vol. 85, pp. 2870-2871, ISSN 0002-7863 (p) 1520-5126 (e)

Keeler, J. (2005) *Understanding NMR spectroscopy*, John Wiley and Sons, Chichester, West Sussex, England, ISBN 0-470-01787-2

Löhr, F. & Rüterjans, H. (1995) (H)NCAHA and (H)CANNH experiments for the determination of vicinal coupling constants related to the ϕ-torsion angle. *Journal of Biomolecular NMR*, Vol. 5, pp. 25-36, ISSN 0925-2738 (p) 1573-5001 (e)

Löhr, F. & Rüterjans, H. (1997) A sensitive method for the measurement of three-bond C',H^{α} *J* coupling in uniformly ^{13}C- and ^{15}N-enriched proteins. *Journal of the American Chemical Society*, Vol. 119, pp. 1468-1469, ISSN 0002-7863 (p) 1520-5126 (e)

Löhr, F., Blümel, M., Schmidt, J.M. & Rüterjans, H. (1997) Application of H(N)CA,CO-E.COSY experiments for calibrating the ϕ-angular dependences of vicinal $J(C'_{i-1},H^{\alpha}_i)$, $J(C'_{i-1},C'_i)$, and $J(C'_{i-1},C^{\beta}_i)$ in proteins. *Journal of Biomolecular NMR*, Vol. 10, pp. 107-118, ISSN 0925-2738 (p) 1573-5001 (e)

Löhr, F., Schmidt J.M. & Rüterjans, H. (1999) Simultaneous measurement of $^3J_{HN,H\alpha}$ and $^3J_{H\alpha,H\beta}$ coupling constants in $^{13}C,^{15}N$-labeled proteins. *Journal of the American Chemical Society*, Vol. 121, pp. 11821-11826, ISSN 0002-7863 (p) 1520-5126 (e)

Löhr, F., Pérez, C., Köhler, R., Rüterjans, H. & Schmidt, J.M. (2000) Heteronuclear relayed E.COSY revisited: Determination of $^3J(H^{\alpha},C^{\gamma})$ couplings in Asx and aromatic residues in proteins. *Journal of Biomolecular NMR*, Vol. 18, pp. 13-22, ISSN 0925-2738 (p) 1573-5001 (e)

Löhr, F., Schmidt, J.M., Maurer, S. & Rüterjans, H. (2001) Improved measurement of $^3J(H^{\alpha}_i, N_{i+1})$ coupling constants in H_2O dissolved proteins. *Journal of Magnetic Resonance*, Vol. 153, pp. 75-81, ISSN 1090-7807

Löhr, F., Reckel, S., Stefer, S., Dötsch, V. & Schmidt, J.M. (2011) Improved accuracy in measuring one-bond and two-bond $^{15}N,^{13}C^{\alpha}$ coupling constants in proteins by double-inphase/antiphase (DIPAP) spectroscopy. *Journal of Biomolecular NMR*, Vol. 50, pp. 167-190, ISSN 0925-2738 (p) 1573-5001 (e)

Martinez-Oyanedel, J., Choe, H.W., Heinemann, U. & Saenger, W. (1991) Ribonuclease T1 with free recognition and catalytic site: Crystal structure analysis at 1.5 Å resolution. *Journal of Molecular Biology*, Vol. 222, pp. 335-352, ISSN 0022-2836

Neuhaus, D. & Williamson, M.P. (1989) *The nuclear Overhauser effect in structural and conformational analysis*, VCH Publishers, New York, ISBN 0-89573-343-9

Pachler, K.G.R. (1963) Nuclear magnetic resonance study of some α-amino acids—I. Coupling constants in alkaline and acidic medium. *Spectrochimica Acta*, Vol. 19, pp. 2085-2092, ISSN 0371-1951

Pachler, K.G.R. (1964) Nuclear magnetic resonance study of some α-amino acids—II. Rotational isomerism. *Spectrochimica Acta*, Vol. 20, pp. 581-587, ISSN 0371-1951

Pérez, C., Löhr, F., Rüterjans, H. & Schmidt, J.M. (2001) Self-consistent Karplus parametrization of ^3J couplings depending on the polypeptide sidechain torsion χ_1. *Journal of the American Chemical Society*, Vol. 123, pp. 7081-7093, ISSN 0002-7863 (p) 1520-5126 (e)

Pervushin, K. (2000) Impact of transverse relaxation optimized spectroscopy (TROSY) on NMR as a technique in structural biology. *Quarterly Reviews of Biophysics*, Vol. 33, pp. 161–197, ISSN 0033-5835

Pfeiffer, S., Karimi-Nejad, Y. & Rüterjans, H. (1996a) Limits of NMR structure determination using variable target function calculations: ribonuclease T1, a case study. *Journal of Molecular Biology*, Vol. 266, pp. 400-423, ISSN 0022-2836

Pfeiffer, S., Engelke, J. & Rüterjans, H. (1996b) Complete ^{1}H, ^{15}N and ^{13}C resonance assignment of ribonuclease T1: Secondary structure and backbone dynamics as derived from the chemical shifts. *Quarterly Magnetic Resonance in Biological Medicine*, Vol. 3, pp. 69-87

Pople, J.A. & Gordon, M. (1967) Molecular orbital theory of the electronic structure of organic compounds. I. Substituent effects and dipole moments. *Journal of the American Chemical Society*, Vol. 89, pp. 4253-4261, ISSN 0002-7863 (p) 1520-5126 (e)

Quaas, R., McKeown, Y., Stanssens, P., Frank, R., Blöcker, H. & Hahn, U. (1988) Expression of the chemically synthesized gene for ribonuclease T1 in Escherichia coli using a secretion cloning vector. *European Journal of Biochemistry*, Vol. 173, pp. 617-622, ISSN 0014-2956 (p), 1432-1033 (e)

Quaas, R., Grunert, H.-P., Kimura, M. & Hahn, U. (1988) Expression of ribonuclease T1 in Escherichia coli and rapid purification of the enzyme. *Nucleosides & Nucleotides*, Vol. 7, pp. 619-623, ISSN 0732-8311

Reif, B., Hennig, M. & Griesinger, C. (1997) Direct measurement of angles between bond vectors in high resolution NMR. *Science*, Vol. 276, pp. 1230-1233, ISSN 0036-8075 (p) 1095-9203 (e)

Reif, B., Diener, A., Hennig, M., Maurer, M. & Griesinger, C. (2000) Cross correlated relaxation for the measurement of angles between tensorial interactions, *Journal of Magnetic Resonance*, Vol. 143, pp. 45-68, ISSN 1090-7807

Roberts, G.C.K. (ed.) (1993) *NMR of macromolecules: A practical approach*, Oxford University Press, Oxford, ISBN 978-0199632244

Schmidt, J.M., Thüring, H., Werner, A., Rüterjans, H., Quaas, R. & Hahn, U. (1991) Two-dimensional ^{1}H,^{15}N-NMR-investigation of uniformly ^{15}N-labeled ribonuclease T1 – Complete assignment of ^{15}N resonances. *European Journal of Biochemistry*, Vol. 197, pp. 643-653, ISSN 0014-2956 (p) 1432-1033 (e)

Schmidt, J.M., Löhr, F. & Rüterjans, H. (1996) Heteronuclear relayed E.COSY applied to the determination of accurate $^{3}J(H^{N},C')$ and $^{3}J(H^{\beta},C')$ coupling constants in *Desulfovibrio vulgaris* flavodoxin. *Journal of Biomolecular NMR*, Vol. 7, pp. 142-152, ISSN 0925-2738 (p) 1573-5001 (e)

Schmidt, J.M. (1997a) Conformational equilibria in polypeptides. I. Determination of accurate $^{3}J_{HC}$ coupling constants in antamanide by 2D NMR multiplet simulation. *Journal of Magnetic Resonance*, Vol. 124, pp. 298-309, ISSN 1090-7807

Schmidt, J.M. (1997b) Conformational equilibria in polypeptides. II. Dihedral-angle distribution in antamanide based on three-bond coupling information. *Journal of Magnetic Resonance*, Vol. 124, pp. 310-322, ISSN 1090-7807

Schmidt, J.M., Blümel, M., Löhr, F. & Rüterjans, H. (1999) Self-consistent ^{3}J coupling analysis for the joint calibration of Karplus coefficients and ϕ-torsion angles. *Journal of Biomolecular NMR*, Vol. 14, pp. 1-12, ISSN 0925-2738 (p) 1573-5001 (e)

Schmidt, J.M. (2007a) A versatile component-coupling model to account for substituent effects. Application to polypeptide ϕ and χ_1 torsion related ^3J data. *Journal of Magnetic Resonance*, Vol. 186, pp. 34-50, ISSN 1090-7807

Schmidt, J.M. (2007b) Asymmetric Karplus curves for the protein side-chain ^3J couplings. *Journal of Biomolecular NMR*, Vol. 37, pp. 287-301, ISSN 0925-2738 (p) 1573-5001 (e)

Schmidt, J.M., Howard, M.J., Maestre-Martínez, M., Pérez, C.S. & Löhr, F. (2009) Variation in protein C^α-related one-bond *J* couplings. *Magnetic Resonance in Chemistry*, Vol. 47, pp. 16-30, ISSN 0749-1581

Schmidt, J.M., Hua, Y. & Löhr, F. (2010) Correlation of ^2J couplings with protein secondary structure. *Proteins*, Vol. 78, pp. 1544-1562, ISSN 0887-3585

Schmidt, J.M., Zhou, S., Rowe, M.L., Howard, M.J., Williamson, R.A. & Löhr, F. (2011) One-bond and two-bond *J* couplings help annotate protein secondary-structure motifs: *J*-coupling indexing applied to human endoplasmic reticulum protein ERp18. *Proteins*, Vol. 79, pp. 428-443, ISSN 0887-3585

Schwalbe, H., Carlomagno, T., Hennig, M., Junker, J., Reif, B., Richter, C. & Griesinger, C. (2001) Cross-correlated relaxtion for measurement of angles between tensorial interactions. *Methods in Enzymology*, Vol. 338, pp. 35-81, ISBN 0-12-182239-7

Spitzner, N., Löhr, F., Pfeiffer, S., Koumanov, A., Karshikov, A. & Rüterjans, H. (2001) Ionization properties of titratable groups in ribonuclease T1 – pKa values in the native state determined by two-dimensional heteronuclear NMR spectroscopy. *European Journal of Biochemistry*, Vol. 30, pp. 186-195, ISSN 0014-2956 (p) 1432-1033 (e)

Tjandra, N. & Bax, A. (1997) Direct measurement of distances and angles in biomolecules by NMR in a dilute liquid crystalline medium. *Science*, Vol. 278, pp. 1111-1114, ISSN 0036-8075 (p) 1095-9203 (e)

Ulrich, E.L., Akutsu, H., Doreleijers, J.F., Harano, Y., Ioannidis, Y.E., Lin, J., Livny, M., Mading, S., Maziuk, D., Miller, Z., Nakatani, E., Schulte, C.F., Tolmie, D.E., Wenger, R.K., Yao, H. & Markley, J.L. (2008) BioMagResBank. *Nucleic Acids Research*, Vol. 36, pp. D402-D408, ISSN 0305-1048 (p) 1362-4962 (e)

Walsh, M.A., McCarthy, A., O'Farrell, P.A., McArdle, P., Cunningham, P.D., Mayhew, S.G. & Higgins, T.M. (1998) X-ray crystal structure of the *Desulfovibrio vulgaris* (Hildenborough) apoflavodoxin-riboflavin complex. *European Journal of Biochemistry*, Vol. 258, pp. 362-371, ISSN 0014-2956 (p) 1432-1033 (e)

Wang, A.C. & Bax, A. (1995) Reparametrization of the Karplus relation for $^3J(H^\alpha\text{-}N)$ and $^3J(H^N\text{-}C')$ in peptides from uniformly $^{13}C/^{15}N$-enriched human ubiquitin. *Journal of the American Chemical Society*, Vol. 118, pp. 1810-1813, ISSN 0002-7863 (p) 1520-5126 (e)

Wang, A.C. & Bax, A. (1996) Determination of the backbone dihedral angle ϕ in human ubiquitin from reparametrized empirical Karplus equations. *Journal of the American Chemical Society*, Vol. 118, pp. 2483-2494, ISSN 0002-7863 (p) 1520-5126 (e)

Watenpaugh, K.D., Sieker, L.C. & Jensen, L.H. (1976) A crystallographic structural study of the oxidation states of Desulfovibrio vulgaris flavodoxin in *Flavins and Flavoproteins* (T.P. Singer ed.), pp. 405-410, Elsevier, Amsterdam, ISBN 0-444-41458-8

Watt, W., Tulinsky, A., Swenson, R.P. & Watenpaugh, K.D. (1991) Comparison of the crystal structures of a flavodoxin in its three oxidation states at cryogenic temperatures. *Journal of Molecular Biology*, Vol. 218, pp. 195-208, ISSN 0022-2836

Wienk, H.L.J., Martínez, M.M., Yalloway, G.N., Schmidt, J.M., Pérez, C., Rüterjans, H. & Löhr, F. (2003) Simultaneous measurement of protein one-bond and two-bond nitrogen-carbon coupling constants using an internally referenced quantitative *J*-correlated [^{15}N,^{1}H]-TROSY-HNC experiment. *Journal of Biomolecular NMR*, Vol. 25, pp. 133-145, ISSN 0925-2738 (p) 1573-5001 (e)

Wüthrich, K. (1986) *NMR of proteins and nucleic acids*, John Wiley and Sons, New York, ISBN 0-471-82893-9

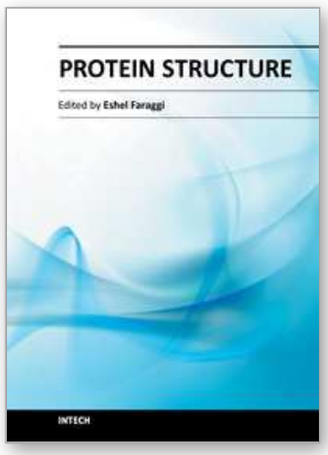

Protein Structure
Edited by Dr. Eshel Faraggi

ISBN 978-953-51-0555-8
Hard cover, 396 pages
Publisher InTech
Published online 20, April, 2012
Published in print edition April, 2012

Since the dawn of recorded history, and probably even before, men and women have been grasping at the mechanisms by which they themselves exist. Only relatively recently, did this grasp yield anything of substance, and only within the last several decades did the proteins play a pivotal role in this existence. In this expose on the topic of protein structure some of the current issues in this scientific field are discussed. The aim is that a non-expert can gain some appreciation for the intricacies involved, and in the current state of affairs. The expert meanwhile, we hope, can gain a deeper understanding of the topic.

How to reference
In order to correctly reference this scholarly work, feel free to copy and paste the following:

Jürgen M. Schmidt and Frank Löhr (2012). Refinement of Protein Tertiary Structure by Using Spin-Spin Coupling Constants from Nuclear Magnetic Resonance Measurements, Protein Structure, Dr. Eshel Faraggi (Ed.), ISBN: 978-953-51-0555-8, InTech, Available from: http://www.intechopen.com/books/protein-structure/refinement-of-protein-tertiary-structure-by-using-spin-spin-coupling-constants-from-nuclear-magnetic

INTECH
open science | open minds

InTech Europe
University Campus STeP Ri
Slavka Krautzeka 83/A
51000 Rijeka, Croatia
Phone: +385 (51) 770 447
Fax: +385 (51) 686 166
www.intechopen.com

InTech China
Unit 405, Office Block, Hotel Equatorial Shanghai
No.65, Yan An Road (West), Shanghai, 200040, China
中国上海市延安西路65号上海国际贵都大饭店办公楼405单元
Phone: +86-21-62489820
Fax: +86-21-62489821

IntechOpen